ELSEVIER

Physica D 86 (1995) 373–395

PHYSICA D

Propagation of population pulses and fronts in a cell replication problem: Non-locality and dependence on the initial function

Alejandro D. Rey[a,*], Michael C. Mackey[b]

[a]*Department of Chemical Engineering, McGill University, 3455 University Street, Montreal, Quebec, Canada H3A 2A7*
[b]*Departments of Physiology, Physics, and Mathematics, and Centre for Nonlinear Dynamics in Physiology and Medicine, McGill University, 3655 Drummond Street, Montreal, Canada H3G 1Y6*

Received 30 August 1994; revised 21 February 1995; accepted 1 March 1995
Communicated by H. Flaschka

Abstract

Here we study the solution types in a simplified equation arising from a cell population dynamics model formulated as a non-linear first order partial differential equation for the cell density $u(t, x)$ in the presence of non-local maturational (x) interactions. This can be considered as a reaction–convection equation in which the cell density is convected with maturation velocity r. The non-local action affects only the reaction (birth) rate. An initial function representing a pulse of small amplitude on an almost extinguished population may be dissipated, may produce multiple pulses, or may remain intact as it travels driven by reaction and convection, depending on the magnitude of the non-local action. Alternately, for localized initial perturbations the equation also has positive traveling front solutions. Positive fronts correspond to the invasion of the zero amplitude solution by a finite amplitude solution. For weak convection ($r \ll 1$, which is the only case treated here) reaction driven fronts arise if the localized initial perturbation acts at a non-zero maturation on the zero amplitude state. A classification arises according to whether the magnitude of the maturation "delay" is larger or smaller than a critical value, and scaling arguments are used to determine the critical delay. For delays larger than critical the reaction driven fronts are oscillatory, and correspond to the case for which the correlation length for non-local action is of the same order as the characteristic length of maturation population gradients that yield oscillatory birth rates. Simulation results are validated and interpreted using scaling arguments and solutions for the local equations.

1. Introduction

Mathematical models for a variety of biological dynamics are most appropriately framed as differential delay [1]. Many of these problems involve descriptions of cell replication, and in this circumstance the natural delay is the cell cycle time.

In previous papers we have considered a model for cell replication in which cells are both proliferating and maturing [2–5]. The dynamics of this situation are described by the solution of a first order partial differential equation [4], in which there is a retardation in the time variable

* To whom all editorial correspondence should be addressed.

0167-2789/95/$09.50 © 1995 Elsevier Science B.V. All rights reserved
SSDI 0167-2789(95)00114-X

as well as non-locality in the maturation variable. The computed dynamics are characterized by a rich variety of spatially homogeneous and inhomogeneous stationary modes, spatially homogeneous oscillating modes, and regular and chaotic traveling wave modes. Many of the time dependent modes were found to be directly associated with a limit cycle solution to the pure birth and death cell population balance equation [3]. More recently [5] this work was extended to the characterization of multiple modes of front propagation under the influence of time delays. The fronts are trajectories connecting the locally unstable zero amplitude cell population state with the locally stable finite amplitude cell population state. One significant finding was the prediction of a front transition that involved reversal of the front motion so the invasion of the zero amplitude solution by the finite amplitude solution was followed by the reverse invasion. Another significant prediction was the presence of a critical delay time above which monotonic fronts bifurcate into oscillatory fronts. The combination of oscillatory fronts and motion reversal phenomena give rise to the formation of a finite spatio-temporal structure.

In this paper we consider a simplified version of the previous model [2,3], in which the delay in the temporal variable is neglected, but the dynamics are still dependent on the spatial non-locality. (Throughout this paper we often use the adjective "spatial" interchangeably with "maturation" for obvious reasons.) This simplification is motivated by our desire to understand the minimal ingredients that yield the various solution features of the more complex model. The essential features of the simplified cell population model are linear convection and non-linear non-local reaction. The growth function in the non-linear non-local reaction, or kinetic term, contains the controlling retardation or delay parameter which is of essential biological relevance. As is well known, reaction–convection systems propagate fronts and pulses [6]. For convection dominated situations, the uniformly moving fronts and pulses are simple translations of the initial data, as predicted by the advection equation. Here we present a characterization of non-locally-induced pattern formation and of the unsteady kinematics of propagating convection-reaction pulses and fronts, predicted by the first order spatially non-local partial differential equation. In Section 2, we present the model equation. In Section 3 we identify two features of pattern formation phenomena for fronts and pulses, and in Section 4 we present our numerical results. The paper concludes with a brief discussion in Section 5.

2. Model cell population equation

A detailed description of the biological significance and mathematical derivation of a cell population model with simultaneous cell replication and maturation, and containing spatial non-locality and temporal retardation has been given in [4]. The governing equations for the cell numbers $u(t, x)$ at time t and (dimensionless) maturation level x are given by

$$\frac{\partial u}{\partial t} + rx\frac{\partial u}{\partial x} = \Delta(u) + \Gamma(u_\alpha)\,, \quad t, x \in \mathbb{R}^+ \times [0, 1]\,, \tag{1}$$

where rx is the (maturation dependent) maturation rate,

$$\Delta(u) = -\delta u \tag{2}$$

is the death function,

$$\Gamma(u) = \gamma u_\alpha(1 - u_\alpha) \tag{3}$$

is the birth rate, and

$$u_\alpha(t, x) \equiv u(t - \alpha, x\,\mathrm{e}^{-r\alpha})\,. \tag{4}$$

[Note the somewhat unusual nature of these dynamics, since the birth rate at (t, x) is a function of the cell numbers at some time $t - \alpha$ in the past, and at a maturation level $x\,\mathrm{e}^{-r\alpha} < x$]. To complete the specification of the problem requires an initial function, taken here as

$$u(t, x) = \varphi(x) , \quad t, x \in [-\alpha, 0] \times [0, 1] . \tag{5}$$

In the present paper, we simplify the model dynamics (1) by neglecting the temporal retardation α in the birth (reaction) function Γ, and also neglect the death term ($\delta = 0$). Without loss of generality we further set $\gamma = 1$. With these modifications the equation investigated in this paper becomes

$$\frac{\partial u}{\partial t} + rx \frac{\partial u}{\partial x} = u_\tau(1 - u_\tau) = \Gamma(u_\tau) ,$$
$$t, x \in \mathbb{R}^+ \times [0, 1] , \tag{6}$$

where $\tau \equiv r\alpha$ and $u_\tau \equiv u(t, x\, e^{-\tau})$, together with the initial function Eq. (5). The magnitude of the maturation delay τ determines the strength of the correlation factor $e^{-\tau}$.

The temporally constant and spatially homogeneous steady states of Eq. (6), defined by $\Gamma(u) \equiv 0$ are given by

$$U_0 \equiv 0 \quad \text{and} \quad U_+ \equiv 1 . \tag{7}$$

Throughout this paper U_0 represents the trivial solution, while U_+ is the spatially homogeneous steady state.

The first objective of this work is to study the propagation of a population pulse, whose shape and motion is controlled by the linear spatially non-homogenous convection (rx) and non-linear non-local reaction effects ($\Gamma(u_\tau)$). In the absence of spatial retardation the amplitude of a pulse will tend to increase (decrease) whenever its amplitude is smaller (larger) than U_+. At a given maturation level x, and in the presence of spatial retardation, a population pulse may increase if $u(t, x\, e^{-\tau}) < 1$ or it may decrease if $u(t, x\, e^{-\tau}) > 1$. Thus it is to be expected that through a cascading effect, a single pulse may act as a localized source, giving rise to a second pulse, which in turn creates a third pulse and so on. As shown below, the end result of non-local generation with a single pulse source is the creation of a train of modulated solitary waves. In addition, the two effects of the linear convection are to first translate the pulse to the right and secondly to disperse it due to the maturation dependence of the convection speed, rx.

The second objective of this work is to study the invasion of one fixed point solution by another through the propagation of a sharp front. The presence of reaction naturally leads to the invasion of the unstable fixed point U_0 by the stable fixed point U_+, here denoted by $U_+ \to U_0$. Following [7] we denote the these fronts as positive. In addition, for sufficiently large values of the delay parameter τ, it will be shown that a front or steep profile induces spatial oscillations on a neighboring uniform U_+ solution, leading to the invasion of U_0 by an oscillatory solution $u(t, x)$, denoted here by $u(t, x) \to U_0$.

Since we wish to study pulse and front propagation, we have focused on initial functions that are time independent localized spatial perturbations of the fixed points. This class of initial functions lead to pulse and front propagation, while initial functions with small gradients usually do not do so [2,3].

The initial function φ_p, used in the numerical section of this work to study pulse propagation represents a localized narrow and small pulse in a nearly extinguished population. We take

$$\varphi_p(x) = \begin{cases} \epsilon , & 0 \le x \le x_1 , \\ a\, e^{-n(x-b)^2} - c , & x_1 < x \le x_2 , \\ \epsilon , & x_2 < x \le 1 , \end{cases} \tag{8}$$

for $t, x \in [-\tau, 0] \times [0, 1]$, where a, b, c, ϵ and $x_{1,2}$ are specified and n satisfies the equation

$$\epsilon = a\, e^{-n(x_i - b)^2} - c , \quad i = 1, 2 , \tag{9}$$

so φ_p is continuous. Other continuous initial functions may be used, but the main phenomena of interest here appear to remain essentially unchanged.

The initial function φ_f that numerically leads to front propagation is one that represents a localized perturbation of the zero amplitude state, whose maximum amplitude lies at $x = 1$:

$$\varphi_f(x) = x^p , \quad t, x \in [-\tau, 0] \times [0, 1] , \quad 1 \ll p . \tag{10}$$

This initial function will be associated with a

propagating front solution corresponding to the invasion of the zero amplitude solution U_0 by the positive amplitude solution U_+, or $U_+ \to U_0$ if τ is less than a critical value, and to the invasion of U_0 by an oscillatory $u(t,x)$ if τ exceeds this critical value. As shown in [5], other front solutions to Eq. (6) exist but they are not considered in this paper.

The boundary condition used in the front propagation study are $u(t, x=0)=0$ for $t>0$, but no boundary condition is enforced in studying pulse propagation.

In the remainder of this paper we study the solutions of Eq. (6) using the two initial functions (8), (10) to obtain insight into the possible modes of pulse and front propagation behavior, and their dependence on the spatial delay τ and the initial function $\varphi(x)$. In examining the occurrence of fronts and pulses, the parameters are fixed throughout except for τ. In both cases, $r=0.01$ (since we only consider the weak convection case $r \ll 1$). For fronts, $p=10$. For pulse solutions we have taken $a=\frac{3}{10}$, $b=\frac{1}{5}$, $c=\frac{1}{10}$, $\epsilon = 10^{-6}$, $x_1 = 0.165$, and $x_2 = 0.235$ so $n \simeq 896.8$. Particular emphasis is placed on the analysis of the pattern formation phenomena induced by the reaction term Γ. Analytical solutions for the unretarded case ($\tau=0$) are used to identify the particular features introduced by spatial retardation. A number of authors [8–13] have studied the global stability properties of a class of differential equations that include Eq. (6) when $\tau=0$. These results indicate that when the initial function satisfies $\varphi(x=0)>0$ the solutions of (6) (with $\tau=0$) will be globally asymptotically stable. However when $\varphi(x=0)=0$ the solutions are chaotic on a function space.

3. Pattern formation phenomena induced by non-linear non-local reactive media

This section presents analytical results that aid in the understanding and confirmation of the numerical solutions to Eq. (6) presented in Section 4, and identifies the intrinsic pattern formation mechanisms operating in any reaction–convection system in which the dynamics are non-local.

In the absence of spatial gradients, the model equation (6) simplifies to the following simple non-linear ordinary differential equation describing the transient kinetics:

$$\frac{\mathrm{d}u}{\mathrm{d}t} = u(1-u)\,. \tag{11}$$

As before, the two steady states of this equation are the trivial solutions $U_0=0$ and the positive solution $U_-=1$. Straightforward considerations shows that the zero amplitude solution U_0 is locally unstable, and the positive amplitude solution U_- is globally stable. This is because for $u=\kappa<1$ we have $\mathrm{d}u/\mathrm{d}t>0$, while for $u=1\pm\kappa$ we have $\mathrm{d}u/\mathrm{d}t<0$ (>0). Thus, with positive initial conditions the solutions always diverge away from U_0, and converge to U_+.

Next we identify two pattern formation mechanisms intrinsic to non-linear non-local reaction: (i) the formation of solitary multiple pulse wave trains when a single pulse is placed on a nearly extinguished population; and (ii) the creation of spatial oscillations when placing a steep population density gradient adjacent to the positive and uniform density U_+.

3.1. Pattern formation mechanism for multiple population pulses

In spatially non-local reactive media, a stagnant source will instantaneously produce a set of secondary sources at locations set by the non-local characteristic length, and with strengths set by the kinetic expression. Because of the non-local nature of the birth, or reaction, term Γ a non-local characteristic length $L_b(x,\tau)$ naturally arises:

$$\Gamma(u_\tau) = \Gamma(t, x - L_b(x,\tau))\,, \tag{12}$$

where

$$L_b(x,\tau) = x(1-\mathrm{e}^{-\tau}) \tag{13}$$

satisfies

$$0 \le L_h(x,\tau) \le 1 - e^{-\tau} . \tag{14}$$

If the delay is $\tau = 1$, the maximum birth rate Γ_{max}, which is at $x_c = \frac{1}{2}$, is a function of the cell density at $x_d = 1/2e \simeq 0.184$ and the correlation distance at x_c is $L_h(x_c, 1) = x_c - x_d \simeq 0.316$. Also, for $\tau = 1$ the correlation distance at $x_c = 1$ is $L_h(x_c = 1, 1) = (1 - e^{-1}) \simeq 0.632$, which is twice as long as at $x_c = \frac{1}{2}$. Clearly, for large τ,

$$0 \le \lim_{\tau \to \infty} L_h(x,\tau) \le 1 . \tag{15}$$

As stated previously, in this paper we study the effects of varying τ and the initial functions on the eventual solution behaviour of Eq. (6), and we interpret these effects through the effect of changes in L_h resulting from the changes in τ. The following analysis identifies the features that control the spatial ordering and the evolution of the secondary sources for the non-local kinetic expression $\Gamma(u_\tau) = u_\tau(1 - u_\tau)$ in the presence of the linear, but non-uniform, convection velocity rx.

In the presence of spatial gradients, integration along the characteristics of Eq. (6) may be employed. Along the characteristics, $x(t) = \xi e^{rt}$, Eq. (6) can be written as

$$\frac{du}{dt} = u_\tau(1 - u_\tau) , \tag{16}$$

where

$$u(t, x(t)) \equiv u(t, \xi e^{rt}) \tag{17}$$

and

$$u_\tau(t, x(t)) \equiv u(t, \xi e^{rt - r\tau}) . \tag{18}$$

ξ is a parameter that defines each characteristic since $x(t = 0) = \xi$, and d/dt denotes the total derivative along the characteristics:

$$\frac{d}{dt} \equiv \frac{\partial}{\partial t} + rx \frac{\partial}{\partial x} . \tag{19}$$

It is useful to consider a set $\{\xi_j\}$ of characteristics correlated in the sense that they obey $\xi_{i+1} = \xi_i e^{\tau}$. In this case the discretized equation (16) is a differential-difference equation given by

$$\frac{du_{j+1}}{dt} = u_j(1 - u_j) , \tag{20}$$

where u_j is the population on the jth characteristic:

$$u_j(t, x_j(t)) \equiv u(t, \xi_j e^{rt}) . \tag{21}$$

In this section we analyze the formation of multiple population pulses when a single initial source pulse is suddenly placed on an extinguished population. Since we are working with a semi-discrete formulation the analysis only yields semi-discrete values of the populations, i.e. $u_j(t)$ on the jth characteristic at time t. At each time t, the discrete population along the characteristics u_j can then be converted to a discrete population on the discrete maturation scale by using $x_j = \xi_j e^{rt}$. We then assume that at $t = 0$

$$u_j(t = 0, x_j) = \begin{cases} M , & j = 0 , \\ U_0 \equiv 0 , & j = 1, \ldots , \end{cases} \tag{22}$$

so a constant source pulse of magnitude M is placed on the U_0 solution at $x_j = x_0$, and wish to determine the response u_j on the $j = 1, 2, \ldots, m$ characteristics. Since M is a known constant, the cell density set $\{u_j\}$, $j = 1, \ldots, m$, follows from successive direct integrations of Eq. (20).

Thus, consider a constant pulse M initially located at $x_0 = \xi_0$. We wish to find the response of the population $u_j(t)$, $j > 1$, whose evolution is governed by Eq. (20), under the following conditions:

$$\xi_{j+1} = \xi_j e^{\tau} , \quad j = 1, 2, \ldots , \tag{23}$$

and

$$u_j(t = 0) \equiv 0 . \tag{24}$$

Setting $u_0 = M$ in Eq. (20) we obtain the governing equation for u_1:

$$\frac{du_1}{dt} = M(1 - M) \tag{25}$$

with the corresponding solution $u_1(t) = \beta t$, where

$$\beta = M(1 - M) . \tag{26}$$

Continuing this process, the equation governing the evolution of $u_2(t)$ is

$$\frac{du_2}{dt} = \beta t(1 - \beta t), \tag{27}$$

with the solution

$$u_2(t) = \beta t[\tfrac{1}{2}t - \tfrac{1}{3}\beta t^2]. \tag{28}$$

Further

$$u_3(t) = \tfrac{1}{6}\beta t^3 - \tfrac{1}{12}\beta^2 t^4 - \tfrac{1}{20}\beta^2 t^5 + \tfrac{1}{18}\beta^3 t^6 - \tfrac{1}{63}\beta^4 t^7. \tag{29}$$

The sequential solutions $\{u_j(t)\}$ for $j = 0, 1, 2, 3$, are shown in Fig. 1 as a function of time t, and the corresponding plots on the fixed maturation scale are shown in Fig. 2.

Fig. 1 shows four cell density amplitudes $u(t, x_j)$ as a function of time, for $M = \frac{1}{10}$, along four characteristics $\{x_j\}$, $j = 1, \ldots, 4$. The figure illustrates how the constant primary source pulse gives rise, through a cascade effect, to a set of secondary pulses. The mth pulse is located on the $\xi_0 e^{mt}$ characteristic. The time dependence of a secondary pulse depends on the initial partial spatial proximity to the primary pulse. The magnitude of the source pulse used here generates a reaction rate smaller than the maximum possible rate ($\Gamma(M) < \Gamma_{max} = \frac{1}{4}$). For this selected magnitude of the source pulse the first ($m = 1$) secondary pulse grows linearly, while the nonlinear growth of each of the subsequent sec-

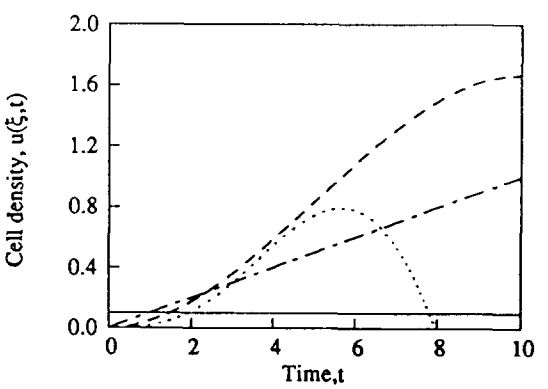

Fig. 1. Multiple pulse response to a single pulse. Cell density $u(t, \xi_j)$ as a function of time, as given by the solution of Eq. (20) for $\tau = 1$ and corresponding to the following characteristics ξ: $\xi_0 = 0.2$ (full line), $\xi_1 = +0.2e^1 = 0.5436$ (dash-dotted line), $\xi_2 = 0.2e^2 = 1.47$ (dashed line), and $\xi_3 = 0.2e^3 = 4.019$ (dotted line). The characteristics are correlated in the sense that $\xi_{j-1} = \xi_j e^{rt}$. The primary pulse ($i = 0$) has a constant amplitude $u_0 = M = 0.1$, and is placed at time $t = 0$ on an extinguished population (i.e. $u_j(t = 0) = 0$, $j > 0$).

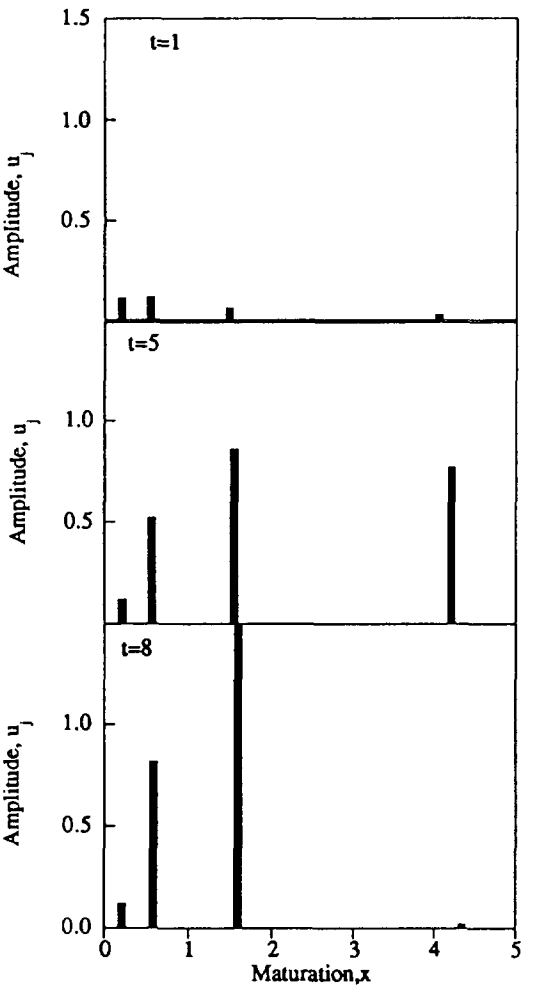

Fig. 2. Dynamics of population pulses. Corresponding cell density amplitudes $u_j(t, x)$ as a function of maturation x, at $t = 1$ (top), $t = 5$) (middle), and $t = 8$ (bottom). Parametric conditions as in Fig. 1. The bars represent the amplitude of the primary and secondary pulses. The constant amplitude primary pulse creates three time dependent secondary pulses. The pulse train is convected to the right, with a maturation dependent velocity (rx). The figure illustrates the operating mechanism for multiple pulse formation, namely, if $u_j < 1$ then $\Gamma(u_{j-1}) > 0$ and u_{j+1} increases, while if $u_j > 1$ then $\Gamma(u_{j-1}) < 0$ and u_{j+1} increases.

ondary pulses ($m \geq 2$) has a maximum at a time that decreases with increasing m. For a given finite time the figure shows a finite number of strictly positive isolated pulses, with a modulated amplitude envelope.

Next we convert the cell density on the jth characteristic $u_j(t, \xi_j e^{j\tau})$ into the density $u_j(t, x_j)$ at maturation x_j, using the method described in the previous paragraph. Fig. 2 shows the corresponding four amplitudes ($\{u_j\}$, $j = 0, 1, 2, 3$) as a function of maturation x for three increasing times. The height of each bar represents the amplitude, with the primary pulse at the left and the third secondary pulse at the right. The effect of convection is to translate the pulses to the right, but the effect is small for the weak convection case illustrated here. As time progresses the fastest growing amplitude is the third mode, and at later stages the fourth and higher modes (not shown) disappear. The time scales are slowed by decreasing the magnitude of the amplitude M of the constant initial source pulse, and many long lasting pulses are found for small M. In this example we neglected the maturation restriction $x \in [0, 1]$, but identical phenomena are found in the unit interval by decreasing the correlation factor $e^{-\tau}$. These particular parametric conditions were chosen to facilitate the understanding of the numerical results in Section 4.1.

By considering a constant source pulse M at a maturation ξ_0, Eq. (20) was amenable to closed form integration along the correlated characteristics (i.e. $\{\xi_j = \xi_0 e^{j\tau}\}$, $j = 1, \ldots, m$). However, in the cases of interest here the initial pulse itself generally evolves under the action of non-linear non-local reaction. When the initial pulse magnitude is not fixed for positive times, analytic integration is not possible, and Eq. (20) becomes a non-linear difference-differential equation. Further, these ideal solutions do not capture the loss of stability of the trivial solution U_0, since the base of the pulses rest on U_0. Below we show that when the primary source pulse rises towards the stable positive U_- solution, a new dissipative mechanism appears that contains the unbounded growth of the first secondary pulse, and thus affects all subsequent pulses. In spite of these idealizations the present results identify the mechanism for the formation of a finite solitary wave train whenever a finite pulse is placed in non-local non-linear reactive media.

3.2. Pattern formation mechanism for oscillatory population fronts

In spatially non-local non-linear reactive media, a steep gradient adjacent to the equilibrium $U_+ = 1$ solution will induce spatial oscillations on this uniform state since neighboring populations will now grow or decay at different rates. The origin of spatially dependent reaction rates is due to the presence of the steep gradient in the driving source. The following analysis identifies the features that control the spatial oscillations about the uniform state U_+ whenever spatial population gradients are found in a neighboring region located within the correlation distance L_h. More precisely, if for $x \geq x_u$ the cell density is uniform and equal to U_+ and if within the interval $L_h(x_u, \tau) \leq x < x_u$ the population gradient is finite ($du/dx \neq 0$), then we show that spatial oscillations can appear in the maturation range $x \geq x_u$ which initially contained the uniform population.

Using the same semidiscrete formulation presented in the previous section, we can understand the mechanism for oscillation formation on U_+ by considering two known constant and unequal source pulses M_1 and M_2 instead of one pulse. We pick the first of these, M_1, such that $\Gamma(M_1) = \Gamma_{\max} = \frac{1}{4}$, so $M_1 = \frac{1}{2}$. The second is selected to be $M_2 = 1$ so $\Gamma(M_2) = 0$. To parallel the numerical simulations shown in Section 4.2 we use the discretized initial function for fronts $\varphi_j(\xi_j) = \xi_j^p$, and momentarily dispense (without loss of generality) with the maturation restriction $x \in [0, 1]$. Given the values of M_1 and M_2, it is easy to determine form the initial function that they are located at $\xi_{0,1} = 0.933$ and $\xi_{0,2} = 1$.

Thus, consider two constant primary pulses

$M_1 = \frac{1}{2}$ and $M_2 = 1$, initially located at $\xi_{0,1} = 0.933$ and $\xi_{0,2} = 1$, respectively. We wish to find the response of the population $u_j(t)$, $j > 1$, whose evolution is governed by Eq. (20), with the initial condition

$$u_j(t=0, x_j) = \begin{cases} M, & j = 0, \\ U_+ \equiv 1, & j = 1, \ldots, \end{cases} \tag{30}$$

and for the following conditions:

$$\xi_{0,1} = e^{-\tau}\,\xi_1 = e^{-2\tau}\,\xi_3 \tag{31}$$

and

$$\xi_{0,2} = e^{-\tau}\,\xi_2 = e^{-2\tau}\,\xi_4, \tag{32}$$

where $u_j(t=0) = 1$, $j = 1, 2, \ldots$.

Note that the cell densities on the odd characteristics $(\xi_1, \xi_3, \ldots)$ are governed by the source $M_1 = \frac{1}{2}$ while the cell densities on the even characteristics $(\xi_2, \xi_4, \ldots)$ are governed by the source $M_2 = 1$. Taking $u_{0,1} = \frac{1}{2}$ in Eq. (20) we obtain the governing equation for u_1:

$$\frac{du_1}{dt} = u_{0,1}(1 - u_{0,1}) \equiv \alpha, \quad u_1(t=0) = 1, \tag{33}$$

whose solution is $u_1(t) = \alpha t + 1$. Substituting $u_1(t)$ in Eq. (20) we obtain the governing equation for u_2:

$$\frac{du_2}{dt} = -\alpha t(\alpha t + 1), \quad u_2(t=0) = 1, \tag{34}$$

whose solution is

$$u_2(t) = 1 - \tfrac{1}{2}\alpha t^2 - \tfrac{1}{12}\alpha^2 t^3. \tag{35}$$

However, if the source is $u_{0,2} = 1$, it will not generate any change since, as we pointed out, the reaction rate is $\Gamma(u_{0,2}) = 0$. Hence, we find that the cell densities along the even characteristics remain constant and equal to 1.

Fig. 3 shows the cell density $u(t, \xi_j)$ as a function of time, along the four characteristics $\{\xi_j\}$, $j = 1, \ldots, 4$. The temporally constant solutions correspond to the even numbered characteristics (ξ_2, ξ_4), the increasing solution corresponds to the first secondary characteristic (ξ_1), and the decreasing solution corresponds to the third secondary characteristic (ξ_3). The figure

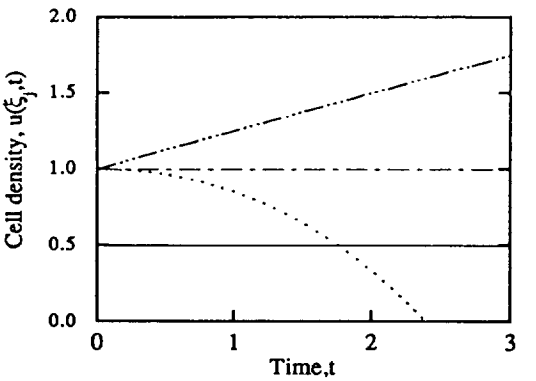

Fig. 3. Oscillatory response to an adjacent gradient on a uniform population. Cell density $u(t, \xi_j)$ as a function of time, as given by Eq. (20), $\tau = 0.08$, and corresponding to the characteristics $\xi_{0,1} = 0.933$ (full line), $\xi_{0,2} = 1$ (dash-dotted line), $\xi_1 = \xi_{0,1} e^{\tau} = 1.01$ (dash-dotted line), $\xi_2 = \xi_{0,2} e^{\tau} = 1.083$ (dash-triple dotted line), and $\xi_3 = \xi_{0,1} e^{2\tau} = 1.094$ (dash-dotted line), and $\xi_4 = \xi_{0,2} e^{2\tau} = 1.173$ (dotted line). The characteristics $\xi_{0,1}$ and $\xi_{0,2}$ correspond to the constant initial source amplitudes, and the characteristics $\{\xi_j\}$, $j = 1,2,3,4$ correspond to the amplitudes we wish to solve for. The characteristics are correlated, such that $\xi_{j+1} = \xi_j e^{jr}$. The two primary amplitudes at $\xi_{0,1}$ and $\xi_{0,2}$ have a constant amplitude $M_1 = \frac{1}{2}$, and $M_2 = 1$, and are placed at time $t = 0$ on a uniform population (i.e. $u_j(t=0) = 1$, $j = 1,2,3,4$). The solution to Eq. (20) gives the evolution of the initially equal amplitudes in response to an adjacent population gradient, represented here by $u_{0,1} = \frac{1}{2}$ and $u_{0,2} = 1$.

shows how a uniform profile U_+ next to a gradient develops spatial oscillations. Locations correlated with U_+ do not grow since the reaction rate is zero, while locations correlated with amplitudes less than unity grow since the growth rate $\Gamma(u_\tau) = u_\tau(1 - u_\tau)$ is positive, and locations correlated with amplitudes larger than unity decay since the growth rate Γ is negative in this region.

The cell density on the jth characteristic, $u_j(t, \xi_j e^{rt})$, can be converted to the density $u_j(t, x_j)$ by using $x_j = \xi_j e^{rt}$. Fig. 4 shows the corresponding six amplitudes $(\{u_j\})$ as a function of maturation x. The length of the bars represents the amplitude, with the first primary pulse at the left and the fourth secondary pulse at the right. The figure shows that the initially uniform

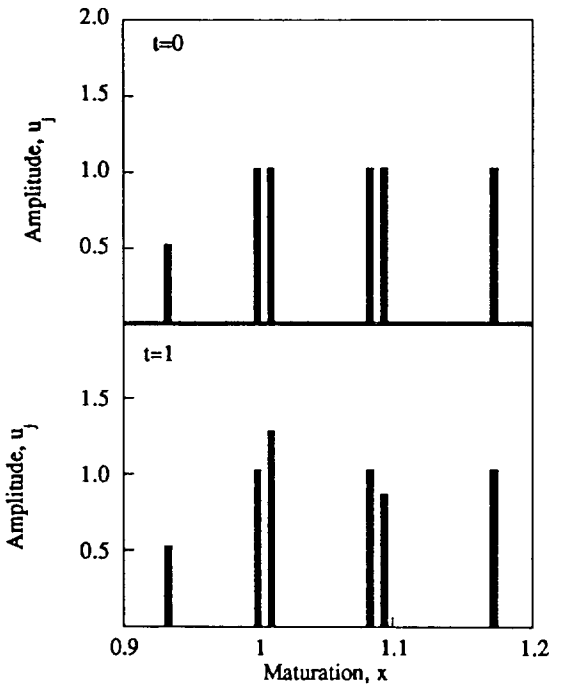

Fig. 4. Dynamics of population pattern formation. Corresponding cell density amplitudes $u_j(t, x)$ as a function of maturation x, at $t = 1$ (top), $t = 5$ (middle), and $t = 8$ (bottom). Parametric conditions as in Fig. 3. The bars represent the amplitude of the primary and secondary amplitudes. At time $t = 0$ the location of the bars is given by the value of ξ, as quoted in Fig. 3. The constant amplitude primary pulses create four time dependent spatially modulated secondary amplitudes. The figure illustrates the operating mechanism for the formation of oscillatory fronts. Namely, a spatial gradient next to a uniform population whose growth rate is affected by non-local effects responds by producing spatial oscillations.

state is replaced by an oscillatory population profile.

By the artifice of imposing two constant source pulses, Eq. (16) is amenable to closed form integration, while in the full retarded case the pulses will generally evolve under the action of non-linear and non-local reaction. In spite of this idealization, the results identify the mechanism for the formation of an oscillatory population density whenever a population gradient is placed adjacent to a spatially uniform non-local non-linear reactive medium.

4. Numerical results and discussion

The reader is referred to [2,3] for a detailed description of numerical methods used in this work as well as their accuracy and validation.

4.1. Scaling and solution regime classification

4.1.1. Definition of time and length scales

The numerical results are naturally classified and explored by considering the relative magnitudes of the operating time and length scales of the problem. The following describes the nature of these scales and their relative magnitudes. As shown below each solution regime corresponds to a particular ordering of the length scales.

A. Time scales. The two time scales operating in Eq. (6) represent the elapsed time for effective change due to convection ($T_c = 1/r$), and by the birth (reaction) rate ($T_b = 1$). Neither of these time scales are changed in this paper. Since $T_b \ll T_c = 1/r$, there is sufficient time for significant reaction induced changes to occur.

B. Length scales. The dynamic length scales of importance in Eq. (6) are: (1) the length scale for convection ($L_c = 1$), which is a consequence of our usual restrictions to the unit maturation interval $x \in [0, 1]$; and (2) the maturation dependent correlation length of the birth rate

$$L_b(x, \tau) = x(1 - e^{-\tau}) . \tag{13}$$

Two additional length scales arise from the initial functions for pulses φ_p and for fronts φ_f, defined in Eqs. (8), (10) respectively.

The characteristic length L_p of the initial perturbation for pulses is taken as the width, or support, of the initial pulse,

$$L_p = x_2 - x_1 , \tag{36}$$

with x_1 and x_2 defined in Eq. (9). This means that for a pulse whose support is centered at x_p the cell population at $x_p \pm L_p/2$ is, at time $t = 0$,

small. The location x_p of the pulse also defines a second characteristic length

$$L_L = 1 - x_p , \tag{37}$$

where

$$x_p = \frac{x_1 + x_2}{2} . \tag{38}$$

The pulse is centered at $x_p = 0.2$ so $L_L = 0.8$. For the chosen values for x_1 and x_2, the characteristic length of the initial pulse is $L_p \simeq 0.07$.

For front propagation two length scales appear. The characteristic length L_f of the initial perturbation for front propagation is defined as the distance from $x = 1$ at which the initial cell population is $u = \frac{1}{2}$:

$$L_f = 1 - (\tfrac{1}{2})^{1/p} . \tag{39}$$

This choice corresponds to the maturation level at which the reaction rate Γ is a maximum ($\Gamma_{\max} = \Gamma(u = \frac{1}{2}) = \frac{1}{4}$). The characteristic length L_d of the initial perturbation for front propagation is the distance from $x = 1$ at which the initial cell population is equal to a number $\rho \ll 1$. The expression for L_d is found directly from Eq. (10) and is given by

$$L_d = 1 - \rho^{1/p} . \tag{40}$$

Here we always take $\rho = 0.01$ and $p = 10$, so the characteristic length is $L_d = 0.369$. For the chosen values, the initial cell population density at the maturation $x = 1 - L_d$ is $\varphi_f(x = \rho^{1/p}) = \rho \ll 1$.

Having identified the dynamic and initial function length scales, we next discuss the possible transition phenomena arising due to changes in their different magnitudes. Recall that in this paper the only length scale that is varied is $L_b(x, \tau)$. For a fixed x, changes in τ may produce length scale ordering reversals, and a consequent transition between solution regimes.

Since we are mainly interested in phenomena occurring in the $[0, 1]$ interval, in this paper the parameters are chosen such that the convection length scale $L_c = 1$ is the largest. For example, the characteristic length for pulses is $L_p = 0.07 < L_c = 1$, and the characteristic length for fronts is $L_f = 0.369 < L_c = 1$. Hence, by changing the retardation parameter τ, the characteristic length $L_b(x, \tau)$ may be larger, smaller, or equal to L_p or L_f. Each of these length scale orderings gives rise to a distinct regime, as discussed below.

4.1.2. *Length scaling and phenomenology of pulse solutions*

The relative magnitude of the length scales gives rise to a range of population pulse phenomenology, schematically shown in Fig. 5. For clarity the sketches are not drawn to scale. The left sketch shows the two length scales L_L and L_p of the initial pulse function $\varphi_p(x)$ (see Eq. (8)). The three sketches in the middle column show the three representative length scale orderings, discussed below. The corresponding three sketches on the right column show the qualitative pulse regime phenomenology corresponding to the length scale orderings shown in the center column. The pulse phenomenology consists of pulse dissipation (PD), and propagation of multiple pulses (MP), and single pulses (SP), as discussed below.

4.1.2.1. Pulse dissipation (PD). $L_c > L_L > L_p/2 > L_b(x = x_p, \tau) > 0$. As the top row of Fig. 5 shows, for pulse dissipation (PD) the correlation length for birth L_b is the smallest. The inequality $L_p/2 > L_b(x = x_p, \tau)$ ensures that the reaction rate Γ at the pulse center x_p depends on a value $u_* = u(x = x_*)$ located within the support of the pulse ($x_1 < x_* < x_p < x_2$). In terms of the delay τ, this regime exists whenever τ lies in a certain delay interval, denoted by $0 \leq \tau \leq \tau_1$. The lower limit corresponds to the unretarded case. A closed form expression for τ_1 is derived in Section 4.2.2. As the delay τ increases the characteristic length L_b increases. For values of the delay τ larger than the critical value τ_1, the inequality $L_p/2 > L_b(x = x_p, \tau)$ fails to hold. In the PD regime, which includes the local kinetics case ($\tau = 0$), no pulses are propagated, and the

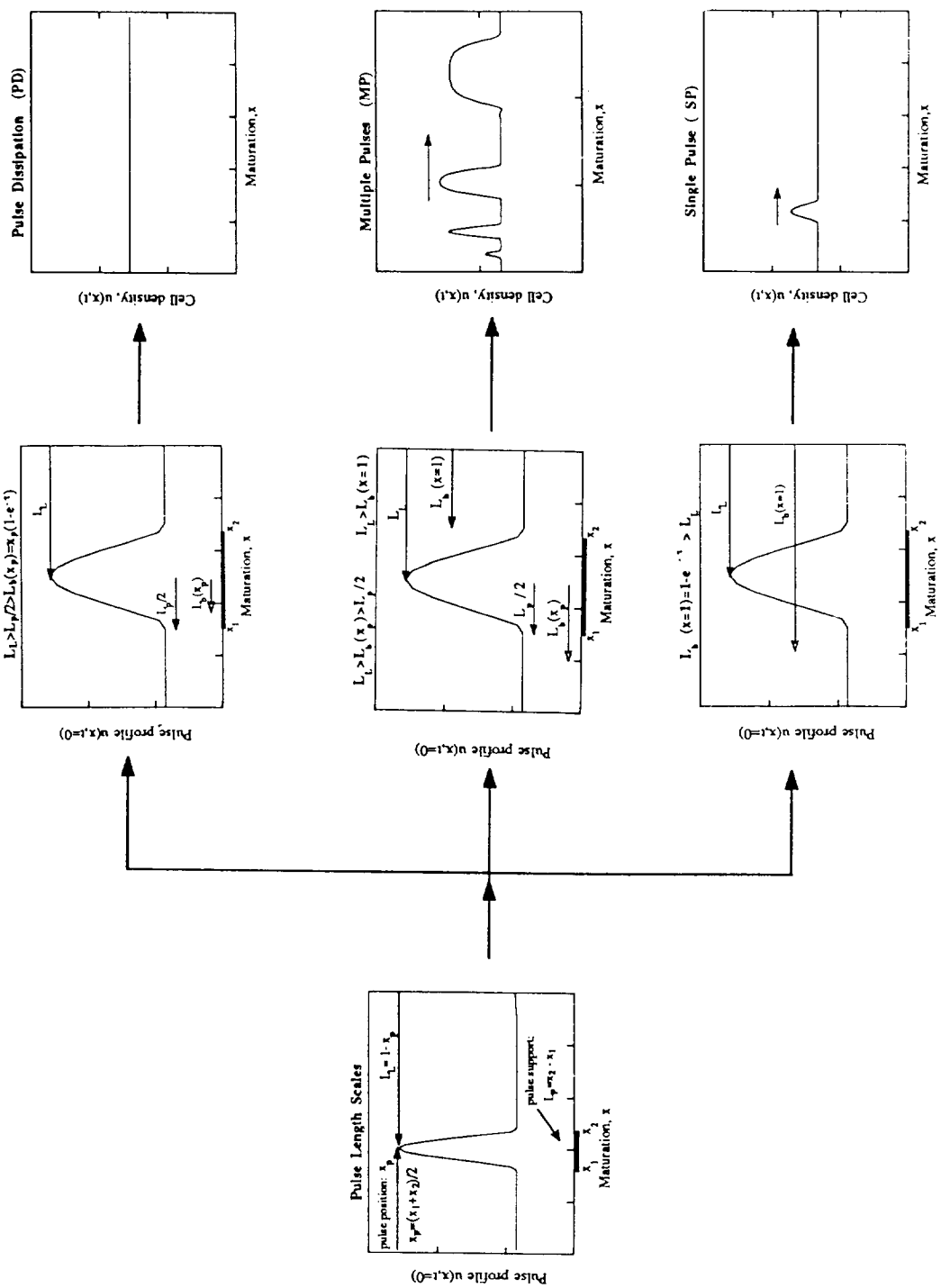

Fig. 5. Schematics of the pulse propagation phenomenology and its relations to the length scale inequalities. The left sketch shows the initial pulse function $\phi_p(x)$ (see Eq. (8)) and its two length scales L_l and L_p. The center column shows the three length scale inequalities that give rise to the pulse propagation regimes shown in the right column. In the pulse dissipation (PD) regime, the initial single pulses dissipates. In the multiple pulse (MP) regime, the single initial pulse gives rise to a train of propagating pulses. In the single pulse (SP) regime, the initial pulse propagates with its shape unchanged.

solutions lead to a uniform population $\lim_{t\to\infty} u(t, x) = U_+$ for $x \in [0, 1]$.

4.1.2.2. Multiple pulse (MP) propagation. $L_c > L_b(x = x_p, \tau) > L_p/2$ *and* $L_c > L_L > L_b(x = 1, \tau)$. The MP regime corresponds to the middle row of Fig. 5. The first set of length scale inequalities ($L_b(x = x_p, \tau) > L_p/2$) ensures that the growth of initial pulse is dictated by the dynamics outside its support (x_1, x_2), and the second set of inequalities ($L_L > L_b(x = 1, \tau)$) guarantees that the initial pulse will affect cell densities whose maturation is less than 1. In terms of the delay τ, this regime defines a second maturation delay interval $\tau_1 \lesssim \tau \lesssim \tau_2$. τ_2 is given in Section 4.2.2. In the MP regime a single initial pulse gives rise to a train of traveling pulses.

4.1.2.3. Single pulse (SP) propagation. $L_c > L_b(x = 1, \tau) > L_L$. The SP regime corresponds to the bottom row of Fig. 5. The length scale inequalities ensures that the initial pulse will not affect cell densities whose maturations are less than one. With respect to τ, this regime is characterized by $\tau_2 \lesssim \tau$ and, as shown below, leads to single (solitary) pulse propagation (SP).

4.1.3. Length scaling and phenomenology of front solutions

The relative magnitude of the length scales gives rise to the front phenomenology shown in Fig. 6. The sketches of the figure are not to scale for clarity. The left sketch identifies the length scales of the initial function $\varphi_f(x)$ (see Eq. (10)). The three sketches in the center column show the three characteristic length scale orderings, discussed below. The three sketches in the right column show the corresponding front phenomenology that appear due to the length scale inequalities shown in the center column. The front phenomenology consists of monotonic fronts (MF), oscillatory fronts (OF), and front dissipation (FD).

4.1.3.1 Monotonic front (MF) propagation. $L_c > L_f > L_b(x = 1, \tau)$. This regime corresponds to the top row sketches of Fig. 6. The correlation length for birth L_b is the smallest. The lower bound of this regime is the unretarded or local model. The inequality $L_f > L_b(x = 1, \tau)$ ensures that the reaction rate in the wake of the front depends on population values that are larger than $u = \frac{1}{2}$, and hence the reaction rate is monotonic. The limiting case included in this regime corresponds to the local model ($\tau = 0$), for which the fronts are always monotonic. Since $L_b(x = 1, \tau) = (1 - e^{-\tau})$ it is useful to write the inequality $L_f > L_b(x = 1, \tau)$ in terms of a delay interval. In terms of τ, this regime defines a maturation delay interval $0 \lesssim \tau \lesssim \tau_3$. τ_3 is given in Section 4.3.2. The critical delay τ_3 defines the upper bound of the delay interval for which monotonic front solutions (MF) exist.

4.1.3.2. Oscillatory front (OF) propagation. $L_c > L_d > L_b(x = 1, \tau) > L_f$. This regime corresponds to the middle row of Fig. 6. The correlation length for birth L_b is larger than that of the front (L_f) but smaller than the length scale L_d. The inequality ensures that the wake of the front will have a birth rate that is non-monotonic, since closer to the front the birth rate will depend on cell densities smaller than $u = \frac{1}{2}$ while farther away from the front the birth rate will depend on cell densities larger than $u = \frac{1}{2}$. Again it proves useful to rewrite the inequalities $L_f < L_b(x = 1, \tau) < L_d$ into a delay interval. In terms of τ this regime corresponds to $\tau_3 \lesssim \tau \lesssim \tau_4$. A closed form expression for τ_4 is given in Section 4.3.4. Whenever the magnitude of the delay τ lies in the interval $\tau_3 \lesssim \tau \lesssim \tau_4$ the non-monotonic reaction rate acting on the wake of the front gives rise to oscillatory front (OF) solutions.

4.1.3.3. Front dissipation. $L_c > L_b(x = 1, \tau) > L_d$. This situation corresponds to the bottom row sketches of Fig. 6. If $L_b(x = 1, \tau)$ is larger than a certain characteristic length L_d insufficient growth occurs, and front extinction occurs. When this occurs, there is insufficient growth to contain

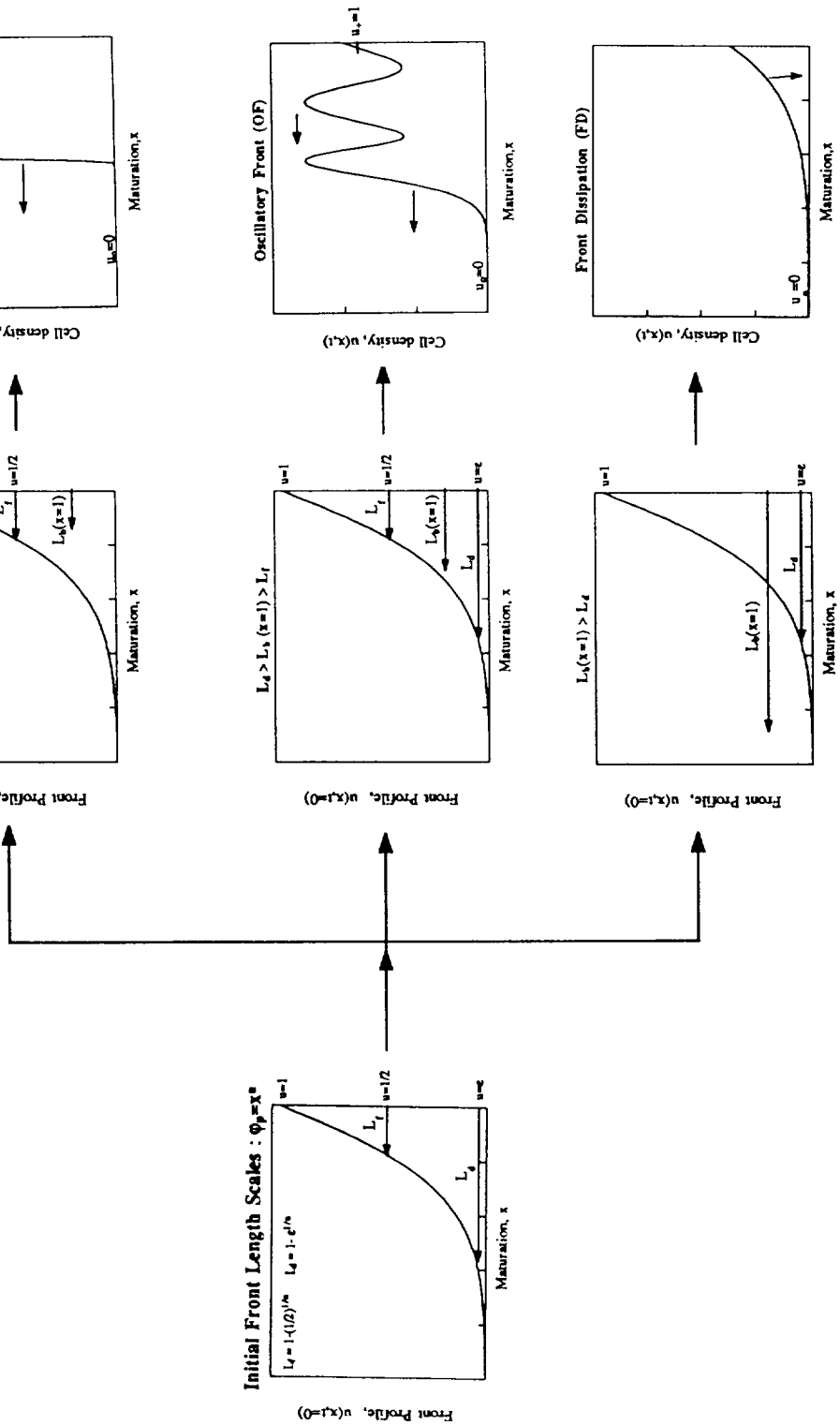

Fig. 6. Schematics of front propagation phenomenology and its relation to the length scale inequalities. The left sketch shows the initial pulse function $\phi_p(x)$ (see Eq. (8)) and its two associated length scales L_L and L_p. The center column displays the length scale inequalities that give rise to the pulse propagation regimes shown in the right column. In the monotonic front (MF) regime, the initial perturbation gives rise to a left moving monotonic front. In the oscillatory front (OF) regime, the initial perturbation gives rise to an oscillatory left moving front. In the front dissipation (FD) regime, the initial perturbation is totally dissipated in a finite time.

the convection and the initial population φ_f will be dissipated. The solution evolves the zero amplitude solution U_0. In terms of the delay, this regime corresponds to $\tau_4 \lesssim \tau$. As shown below, for values of the delay larger than τ_4 fronts will not propagate.

Table 1 presents a compact summary of the different pulse and front propagation regimes shown in Figs. 5, 6, defines the nomenclature, and gives the corresponding parametric conditions in terms of the initial function ($\varphi(x)$), length scale ordering, and the spatial delay (τ). The last column shows the figure numbers showing the computed solutions to Eq. (6) for the different regimes.

4.2. Pulse propagation

Pulses are driven by both convection and reaction. Convection translates the pulse along the increasing maturation direction. In addition since the zero amplitude solution U_0 is unstable, reaction drives the whole profile upwards and towards the locally stable U_+ solution on the faster time scale $T_b = 1$. For relatively small delays such that $0 \lesssim \tau \lesssim \tau_1$, the original pulse φ_p dissipates. On the other hand, for relatively strong delays with $\tau_1 \lesssim \tau \lesssim \tau_2$, multiple pulses arise in the interval [0, 1], and propagate driven by reaction–convection. Lastly, when $\tau_2 \lesssim \tau$, no secondary pulse forms in [0, 1], and only a single pulse propagates. The last two regimes are in agreement with the predictions of Section 3.1. Below we present numerical evidence for these behaviors and provide further explanations for their existence. Analytical results for the unretarded case ($\tau = 0$) provide a useful reference.

4.2.1. Analytical solutions for unretarded reaction ($\tau = 0$)

For small τ, the solution of (6) with $\tau = 0$ provides a good asymptotic approximation to the solution, and gives insight into the solution behavior for non-zero $\tau \lesssim \tau_1$. Using the method of characteristics we obtain, for $\tau = 0$ and a general initial function $\varphi_p(x)$, the following solution to Eq. (6):

Table 1
Classification of pulse and front solutions and parametric conditions

Solution type	Regime type (symbol)	Initial function $\varphi(x)$ $0 \le x \le 1$ $t = 0$	Ordering of length scales (L_i)	Spatial delay interval (τ)	Figure number(s)
Pulses (P)	pulse dissipation (PD)	φ_p Eq. (8)	$L_c > L_L > L_p/2 > L_b$	$0 \le \tau < \tau_1$	7
	multiple pulses (MP)	φ_p Eq. (8)	$L_c > L_L > L_p/2$ & $L_c > L_L > L_b$	$\tau_1 \le \tau < \tau_2$	8,9
	single pulse (SP)	φ_p Eq. (8)	$L_c > L_b > L_L$	$\tau > \tau_2$	10
fronts (F)	$U_+ \to U_0$ monotonic fronts (MF)	$\varphi_f = x^n$ $n = 10$	$L_c > L_f > L_b$	$0 \le \tau < \tau_3$	13
	$u(t, x) \to U_0$ oscillatory fronts (OF)	$\varphi_f = x^n$ $n = 10$	$L_c > L_d > L_b > L_t$	$\tau_3 < \tau < \tau_4$	15
	$u(t, x) \to 0$ front dissipation (FD)	$\varphi_f = x^n$ $n = 10$	$L_c > L_b > L_d$	$\tau > \tau_4$	16

$$u(t,x)=\frac{\varphi_p(x\,\mathrm{e}^{-t})\,\mathrm{e}^{t}}{1+\varphi_p(x\,\mathrm{e}^{-t})(\mathrm{e}^{t}-1)}. \tag{41}$$

It is clear from Eq. (41) that $\lim_{t\to\infty} u(x,t)=U_+$ for $\varphi_p(0)>0$.

Fig. 7 shows the cell density as a function of maturation as given by Eq. (41) for φ_p given by Eq. (8) at four different times. The initial pulse quickly grows driven by reaction until it reaches U_+. The time scale for the reaction driven growth ($T_b=1$) is smaller than the time scale for the lateral convection driven motion ($T_c=1/r>1$). The rest of the (initially nearly extinguished) population lags behind the faster growing initial pulse but eventually reaches U_+. The slow convection has no significant effect on the location of the dissipating pulse.

4.2.2. *Numerical solutions for multiple pulse propagation (MP)*

The parametric conditions for multiple pulse propagation are $\tau_1\lesssim\tau\lesssim\tau_2$ (see the second row in Table 1). The numerical approximations to τ_1 and τ_2 are obtained in the next two paragraphs. As mentioned above, the value of $\tau_1(\tau_2)$ defines the lower bound (upper bound) of the delay interval for which multiple pulse solutions exist. Whenever $\tau\lesssim\tau_1$, pulse propagation does not occur. We found that for small delays ($\tau\ll\tau_1$) Eq. (41) gives a good approximation to the numerically computed solutions. Although we have been unable to determine the exact threshold τ_1 below which pulses do not form and propagate, a simple length scaling gives a good approximation.

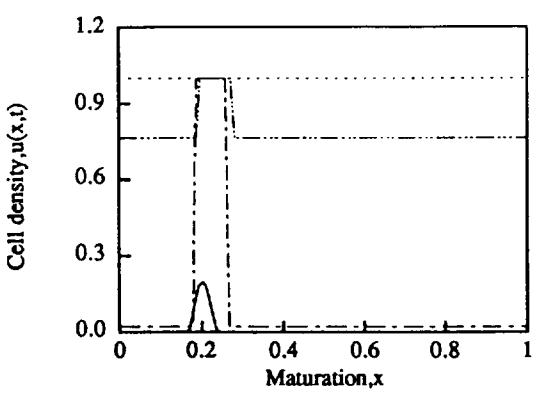

Fig. 7. Population pulse dissipation. Analytically computed cell density $u(t,x)$ with $\tau=0$ as a function of maturation for $t=0$ (full line), $t=10$ (dash-dotted line), $t=15$ (dash-triple dotted line), and $t=20$ (dotted line). The initial pulse is given by Eq. (8). The profiles are found from Eq. (41). At early times the pulse grows up to $U_+=1$, and the rest of the population trails behind. At sufficiently long times the pulse disappears and the population is uniform and equal to U_+. Simulation show that for small delays such that $\tau>\tau_1=0.193$, Eq. (41) gives a good approximation to the numerically computed behavior, and multiples or single pulses do not propagate.

If at the initial pulse location (x_p) the nonlocal correlation length $L_b(x_p,\tau)$ of (13) is set equal to half of the pulse base $L_p/2$ given by (36), the critical delay τ_1 is found to be

$$\tau_1\simeq\ln\left(\frac{x_p}{x_1}\right), \tag{42}$$

where we also used (38). For the selected values, $\tau_1=0.193$. This condition ensures that the pulse will not overshoot U_+, as in Fig. 7, and also ensures that no secondary peak forms.

A similar length scaling argument is used to approximate the critical delay τ_2 above which only a single peak propagates in the interval $[0,1]$. An approximate expression for the critical delay τ_2 is obtained when the maximum correlation length $L_b(x=1,\tau)$ at the unit maturation is equal to the pulse distance from $x=1$, given by L_L from (37). Since

$$L_b(x=1,\tau)=1-\mathrm{e}^{-\tau} \tag{43}$$

we obtain

$$\tau_2\simeq\ln\left(\frac{1}{x_p}\right), \tag{44}$$

which gives $\tau_2=1.60$. Next we show typical numerical results in the interval $\tau_1<\tau<\tau_2$ that illustrate multiple pulse propagation.

Fig. 8 shows the numerically computed cell density $u(t,x)$ as a function of maturation x, for two different delays and several times. For smaller delays (top), multiple propagating pulses

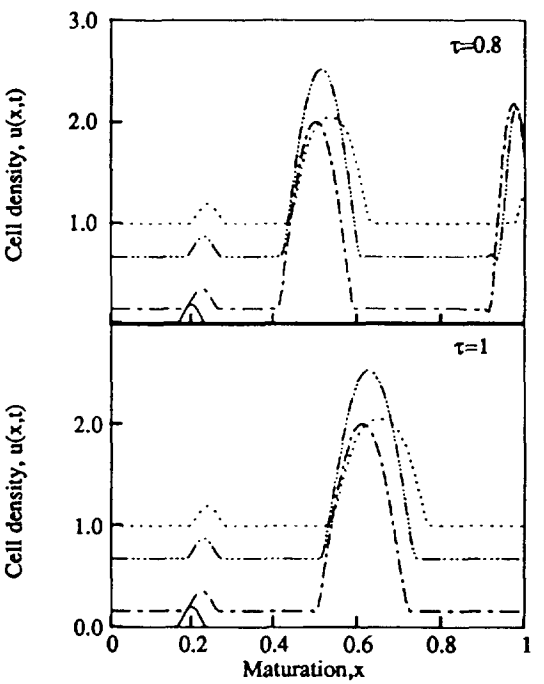

Fig. 8. Generation and propagation of a train of population pulses. Cell density $u(t, x)$ as a function of maturation x, for $\tau = 0.8$ (top) and $\tau = 1$ (bottom) at $t = 0$ (full line), $t = 10$ (dash-dotted line), $t = 15$ (dash-triple dotted line), and $t = 20$ (dotted line). This figure shows a typical multiple pulse (MP) solution. The initial pulse produces two secondary pulses. Multiple pulses form whenever $\tau_1 = 0.193 < \tau < \tau_2 = 1.6$. The pulses are driven to the right by convection, and upwards by reaction. The origin of the secondary pulse lies in the non-local reaction rate. The number (m) of pulses that may appear in the $0 \leq x \leq 1$ interval depends on the correlation length for non-local growth at the location x_p of the initial source pulse, and is given in Eq. (47). For the top plot Eq. (47) predicts $m = 2$, and for the bottom plot it predicts $m = 1$, in accordance with the simulations.

are found in agreement with the results of Section 3.1. For larger delays (bottom), only one secondary pulse forms and propagates. The effect of the delay magnitude on the number of secondary pulses that are born and propagate is given by the integral number of correlation lengths that fit into the unit interval. To find the integral number m of secondary pulses initially formed in the interval $[0, 1]$, we first calculate the maturation levels x_i that are correlated with x_p for a given τ using

$$x_p = x_i \, e^{i\tau}, \quad i = 1, \ldots, m, \tag{45}$$

and then find the maximum maturation of the set of correlated locations that lies in the interval from

$$x_p \, e^{m\tau} = 1, \tag{46}$$

or

$$m = \text{int}\left[\frac{1}{\tau} \ln\left(\frac{1}{x_p}\right)\right], \quad \tau_1 \lesssim \tau \lesssim \tau_2, \tag{47}$$

where int$[x]$ denotes the largest integer such that int$[x] \lesssim x$. For the upper part of Fig. 6, $\tau = 0.8$ to predict that $m = 2$, and for the lower part of Fig. 6 $\tau = 1$ to $m = 1$. The scaling criteria (42), (44), (47) are thus in agreement with the simulations.

Fig. 8 also shows the separate effects of reaction and convection. The reaction drives the populations upwards toward $U_+ = 1$, while convection drives the pulses laterally to the right. At the latest time shown the initial primary pulse remains intact due to the fact that the reaction rate at the pulse is zero due to non-locality. Comparing this result with the late stage shown in Fig. 7, we see that for non-local reaction the primary pulse survives but for local reaction it disappears, as dictated by the evolution of the birth rate at the pulse's maturation. Since the primary pulse survives intact, this source provides for the continuous dissipation of the secondary pulse. In overshooting U_+ the pulse generates a negative growth rate. This feature is shown by comparing the profiles for the last two times in both plots of Fig. 8. In certain cases the continued dissipation of the first secondary pulse eventually leads to negative cell numbers on $[0, 1]$, and therefore to non-physical results. Nonnegative and finite cell numbers are obtainable with a different reaction source term Γ such that $\Gamma(u) \geq 0$, $\Gamma(0) = 0$, and $\lim_{u \to \infty} \Gamma(u) = 0$.

The dispersion effect seen in Fig. 8 is a direct consequence of the fact that the distance between characteristics $x = \xi \, e^{rt}$ increases with increasing time. Thus a narrow pulse will broaden

through convection. An additional dispersive effect is contained in the reaction term, since its correlation length $L_b = x(1 - e^{-\tau})$ increases with increasing maturation. This dispersion effect is clearly seen in Fig. 9 which shows the cell population density $u(t, x)$ as a function of x, for $\tau = 0.8$ at $t = 4$. The maturation scale is extended beyond $x = 1$ for clarity and illustrates that dispersion increases for increasing maturation.

4.2.3. *Numerical solutions for single pulse solutions (SP)*

The parametric conditions for single pulse propagation are $1.6 \simeq \tau_2 \lesssim \tau$. If the delay is sufficiently large the reaction rate at any maturation value in the unit interval is dictated by the population density at $x = 0$, that is $\Gamma(u(t, 0))$. In the infinite τ limit the governing equation (6) simplifies to

$$\frac{\partial u}{\partial t} + rx\frac{\partial u}{\partial x} = \Gamma(u(t, 0)) \,. \tag{48}$$

which is a linear wave equation with a time dependent source. Thus we may expect that the initial function φ_p increases uniformly towards U_+ as it is convected to the right in the maturation scale. When the boundary population reaches U_+ the growth stops.

Fig. 10 shows the cell density $u(t, x)$ as a function of maturation x, for four times and $\tau = 10$. For this delay the effect of the initial pulse is located at $x = x_p e^{10} > 1$, and its presence will have no effect on the cell population in the $[0, 1]$. The figure shows that the pulse is driven upward by reaction, and (slowly) to the right by convection. It is interesting to note that for very large delays, the initial population non-uniformities are "frozen in" and neither evolve or decay.

4.3. *Reaction fronts*

The last two rows in Table 1 correspond to reaction fronts (F), driven by reaction. Since U_0

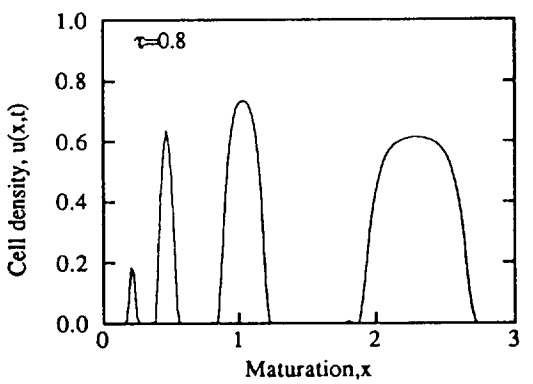

Fig. 9. Population dispersion phenomena. Cell population density $u(t, x)$ as a function of maturation x for $\tau = 0.8$ at time $t = 4$. The maturation interval is extended past $x = 1$ to illustrate pulse dispersion. The origin of the pulse dispersion is twofold. Due to the maturation dependent convection velocity (rx) the characteristics are non-linear $(x = \xi e^{rt})$, which produces an increasing distance between neighboring characteristics for increasing times. The second effect is due to the maturation dependence of the correlation length. $L_b(x, \tau) = x(1 - e^{-\tau})$, for non-local generation. Since L_b increases as the maturation x increases a narrow peak centered at x_p and of support (base thickness) $x_2 - x_1$, will produce a pulse centered at $x_p + L_b(x_p, \tau)$ and of wider support $(x_2 - x_1)e^{\tau} > x_2 - x_1$.

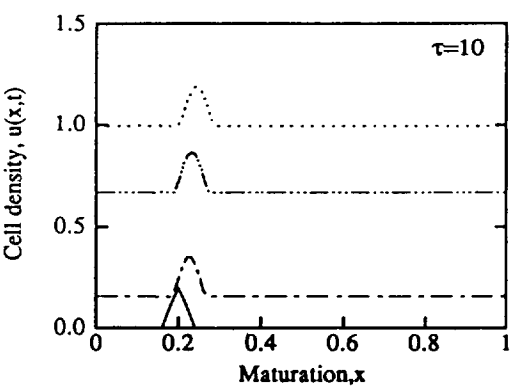

Fig. 10. Solitary population pulse propagation. Cell density $u(t, x)$ as a function of maturation x, $\tau = 10$. The corresponding times are $t = 0$ (full line), $t = 12$ (dash-dotted line), $t = 14.4$ (dash-triple dotted line), and $t = 19.2$ (dotted line). This figure shows a typical single pulse (SP) solution. Since $\tau > \tau_2 \simeq 1.6$, multiple pulses do not form in the $0 \le x \le 1$ interval, and single traveling pulse solutions are found. This is predicted by Eq. (47). The shown pulse amplitude does not dissipate, and its amplitude remains constant. The initial pulse is driven to the right by convection and upwards by reaction. In the infinite delay case Eq. (3) becomes a linear wave equation with a time dependent source (Eq. (48)).

is unstable, it will be invaded by a finite amplitude solution and the resulting positive front will move left in the x direction. Further, since the characteristic at $x = 0$ does not carry information into the $x > 0$ region, the U_0 solution is not convected in the positive x direction. [For constant convection, where rx is replaced by r, the characteristics are linear, and the characteristic passing through $x = 0$ will convect the U_0 into the $x > 0$ range. This last case was investigated in [5] and gives rise to reversal of front motion.]

In the present paper the convection velocity (rx) is maturation dependent and front reversal does not occur. The front kinematics are time dependent, since the front accelerates from rest and decelerates as it approaches the impermeable $x = 0$ boundary. For relatively weak delays, $\tau \lesssim \tau_3$, the positive monotonic fronts (MF) correspond to the invasion of U_0 by U_+. On the other hand, for larger delays such that $\tau_3 \lesssim \tau \lesssim \tau_4$, the positive oscillatory fronts (OF) correspond to the invasion of the zero amplitude solution U_0 by a time dependent spatially non-homogeneous solution $u(t, x)$. The non-local source of spatial oscillations was identified in Section 3.2, using a simplified analysis. Finally, if the delay τ is larger than τ_4, the initial perturbation dissipates and the solution evolves towards U_0. Below we present numerically computed population front solutions and provide further explanations for various front phenomena.

4.3.1. *Analytical solutions for unretarded reaction fronts* ($\tau = 0$)

Again $\tau = 0$ (see fourth row in Table 1). For sufficiently small delays, the solution of Eq. (6) with $\tau = 0$ provides a good asymptotic approximation. The solution is identical with (41) after replacing φ_p by φ_f:

$$u(t, x) = \frac{\varphi_f(x\,\mathrm{e}^{-rt})\,\mathrm{e}^{t}}{1 + \varphi_f(x\,\mathrm{e}^{-rt})(\mathrm{e}^{t} - 1)}, \tag{49}$$

where $\varphi_f(x) = x^p$ for $x \in [0, 1]$. Fig. 11 shows the cell density $u(x, t)$, given by (49), as a function of maturation x, for five increasing times. As the front translates to the left it steepens and its velocity decreases. The evolution of the front's steepness is dictated by the position dependent reaction rate $\Gamma(u)$. At $u = \frac{1}{2}$, the reaction rate is largest, while $\lim_{u \to 0,1} \Gamma(u) = 0$.

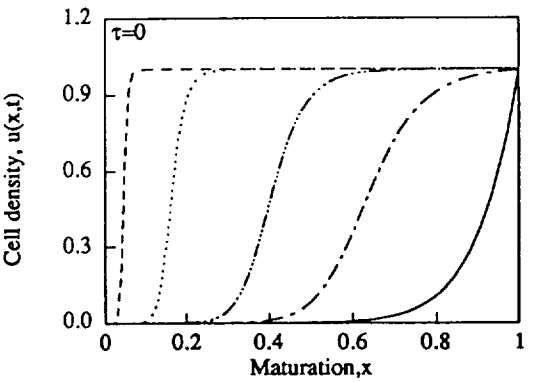

Fig. 11. Population front propagation. Cell density $u(t, x)$ as a function of maturation x for $p = 10$, and for four times $t = 0$ (full line), $t = 5$ (dash-dotted line), $t = 10$ (dash-triple dotted line), $t = 20$ (dotted line), and $t = 35$ (dashed line), as predicted by Eq. (49). The wake of the front is monotonic. As it moves to the left, the front steepness increases and its velocity decreases.

To understand the driving forces governing the front kinematics we again define the front location x_* as the maturation level at which $u(t, x_*) = \frac{1}{2}$. With this definition, Eq. (49) predicts that the front position x_* is given by the following ratio of the convection dependent contribution to the reaction dependent contribution:

$$x_*(t) = \frac{\mathrm{e}^{rt}}{[1 + \mathrm{e}^{t}]^{(1/p)}}. \tag{50}$$

This shows how the convection (numerator) tends to translate the front to the right while reaction (denominator) tends to translate the front to the left. For the parameters we chose, at early times reaction has a slightly larger magnitude than convection. As time increases the reaction effect increases at a faster rate than the convection effect so at later times reaction dominates, resulting in the motion of the front in the direction of decreasing maturation. The front velocity $\mathrm{d}x_*/\mathrm{d}t$ is given from Eq. (50) by

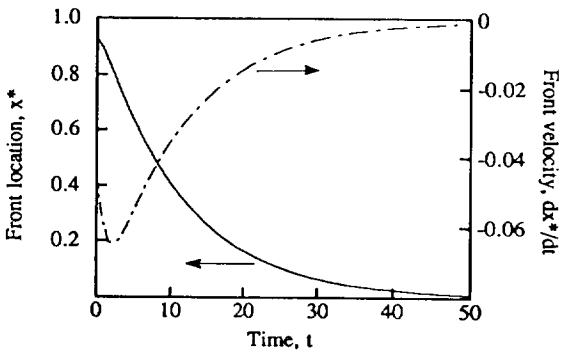

Fig. 12. Population front kinematics. Front position x_* and corresponding front velocity dx_*/dt as a function of time, for $\tau = 0$. The front position x_* is given by Eq. (50) and the front velocity dx_*/dt by Eq. (51). After an initial increase, the front velocity decreases exponentially towards zero.

$$\frac{dx_*}{dt} = \frac{e^{rt}}{[1+e^t]^{(1-p)}}\left[r - \frac{1}{p(1-e^t)}\right]. \tag{51}$$

Fig. 12 shows the front position x_* as a function of time (full line) and the front velocity dx_*/dt as a function of time (dashed-totted line). The arrows indicate the corresponding axes. After the initial transient the velocity of the front decreases exponentially. As expected,

$$\lim_{t\to\infty} x_* = \lim_{t\to\infty} \frac{dx_*}{dt} = 0. \tag{52}$$

4.3.2. Numerical solutions for monotonic reaction fronts (F)

The parametric conditions for the present regime is $0 \le \tau \lesssim \tau_3$ (see fourth row in Table 1). The approximation to τ_3 is derived in the next paragraph. In this regime we find monotonic fronts, and if τ is sufficiently small we expect that Eq. (49) will provide a good approximation to the solution. Fig. 13 shows the computed cell density $u(t,x)$ as a function of maturation x for three different times. For small delays, the fronts are heteroclinic trajectories between U_0 and U_-. Although no analytical results, as given by Eq. (49), are available for front kinematics when $\tau \neq 0$, the simulations seem to indicate that the delay only modifies the reaction contribution to the front motion and this contribution controls

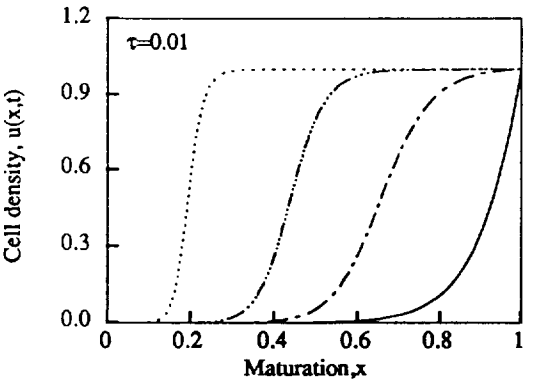

Fig. 13. Monotonic front propagation. Cell density $u(t,x)$ as a function of maturation x (full line) for $\tau = 0.01 < \tau_3 \simeq 0.069$. The corresponding times are: $t = 0$ (full line), $t = 5$ (dash-dotted line), $t = 10$ (dash-triple dotted line), and $t = 20$ (dashed line). For small spatial delays the finite amplitude side ($x > x_-$) of the front remains monotonic.

the front motion as τ increases. The delay effect on kinematics will be discussed further in the next section, where stronger delay regimes are discussed.

An exact expression for τ_3, which defines the upper bound of the delay interval for which fronts remain monotonic was not found, but length scaling arguments again provide a useful approximation. In Section 3.2 we found that placing a gradient next to the uniform U_+ state results in spatial oscillations in the homogeneous population. If L_f is the characteristic length for the initial front solution and $L_b(x)$ the correlation length for non-local effect, then when $L_b < L_f$, the birth rate acting on U_+ on the maturation interval $[x, x + L_b]$ will be monotonic and oscillations will not form. Following this scaling argument, and using (39) and (43), we obtain an expression for τ_3:

$$\tau_3 \simeq \frac{\ln 2}{p}. \tag{53}$$

For $p = 10$ this predicts that $\tau_3 \simeq 0.0693$. This is consistent with the numerical simulation since, as shown in Fig. 15, for $\tau = 0.08 > \tau_3 \simeq 0.0693$ the front is strongly oscillatory and, as shown in Fig. 13, for $\tau = 0.01 < \tau_3$ the front is monotonic.

4.3.3. Numerical solutions for oscillatory reaction fronts (OF)

The parametric condition for these fronts is $\tau_3 \lesssim \tau \lesssim \tau_4$ (see fifth row in Table 1). As mentioned above, the value of $\tau_3(\tau_4)$ defines the lower bound (upper bound) of the delay interval for which oscillatory front (OF) solutions exist. As shown in Section 3.2 sharp gradients next to U_+ produce oscillations on a uniform homogeneous population. In addition to introducing oscillations, increasing the magnitude of the delay will decrease the front velocity. For sufficiently large delays the initial perturbation will be dissipated and fronts will not propagate. In what follows we characterize the front's velocity dependence on delay magnitude, and provide numerical evidence for oscillatory population fronts.

An estimate of τ_4 is found by requiring that the correlation length for non-local action at $x = 1$ be of the same magnitude as the characteristic length at which the initial perturbation $\varphi_f = x^p$ yields infinitesimal growth. Infinitesimal growth occurs when the initial cell population is vanishingly small, $\varphi_f = \rho = x^p \ll 1$. If $L_b(x = 1, \tau) = 1 - e^{-\tau}$ is the correlation length for non-local action at $x = 1$ and $L_d = 1 - \rho^{1/n}$ defines the length at which there is infinitesimal growth, the critical threshold τ_4 of the spatial delay above which the initial perturbation is dissipated is given by

$$\tau_4 \simeq \frac{1}{p} \ln \frac{1}{\rho}. \tag{54}$$

For $p = 10$ and $\rho = 1/100$, we have $\tau_4 \simeq 0.46$. This result is in good agreement with the simulations. For example, Fig. 16 corresponds to $\tau = 1 > \tau_4 = 0.46$, and the evolutions of the profiles are consistent with the predicted front dissipation.

Fig. 14 shows the computed front position x_* as a function of time four different delays. The full line represents the unretarded case ($\tau = 0$). The figures clearly show the trends for increasing delay magnitudes. For small delays, departures from the unretarded case are small, but increase with increasing retardation. Increasing delay magnitudes decrease the front velocity. As the delay $\tau \to \tau_4$, the front velocity decreases to zero, and we obtain a regime of slow moving fronts. For values of $\tau > \tau_4$ fronts will not penetrate into the maturation range $x < 1$.

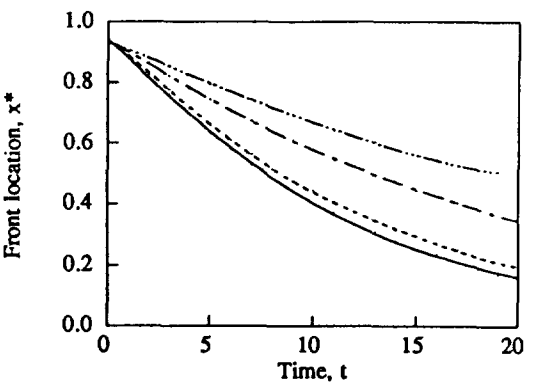

Fig. 14. Dissipative non-local effects on population front kinematics. Front location x_* as a function of time t, for four increasing delays $\tau = 0$ (full line), $\tau = 0.01$ (dashed line), $\tau = 0.05$ (dashed dot line), and $\tau = 0.08$ (dashed triple dot line). The front location x_* is defined as the maturation level at which the cell density is $u = \frac{1}{2}$. As the delay increases the front velocity decreases at all maturation levels. As $\tau \to \tau_4 \simeq 0.46$, the front velocity decreases to zero. For $\tau > \tau_4$ fronts do not propagate.

Fig. 15 shows the cell density $u(t, x)$ as a function of maturation x for $\tau_3 < \tau = 0.08 < \tau_4$, and four different times. For $\tau > \tau_3$ the gradients produce oscillations and the simulations clearly reflect this fact. We have performed extensive computations for this regime and Fig. 15 is representative. Similar types of oscillatory fronts can be found in other reaction–diffusion models [14], in the KdV equation [15], and in the solutions to Eq. (1) in the absence of spatial delays [5]. The wave length of the pattern depends on τ and p, since these two parameters control the length scales that give rise to the phenomenon. As the front travels, the wave length of the leading oscillation decreases. This reflects the fact that as the steepness of the perturbation (front) that produces the oscillation

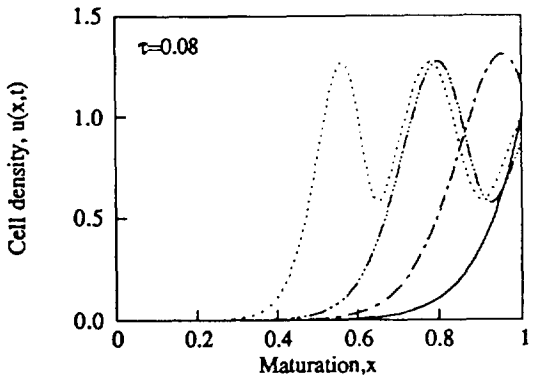

Fig. 15. Oscillatory population fronts. Cell density $u(t,x)$ as a function of maturation x (full line), for $\tau_3 \simeq 0.069 < \tau = 0.08 < \tau_4 \simeq 0.46$. The figure shows a typical oscillatory front (OF) solution. The wake of the front displays spatial oscillations. The origin of the oscillations was explained in conjunction with Fig. 4. A gradient next to a uniform population tend to produce oscillations.

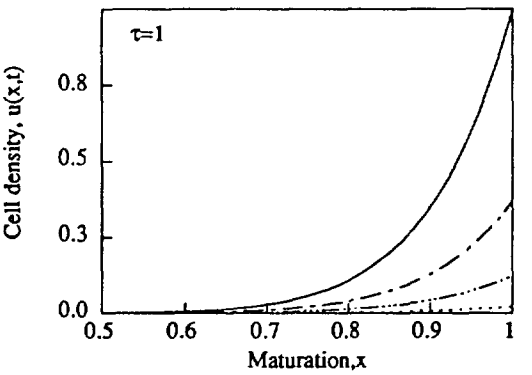

Fig. 16. Dissipation of population fronts. Cell density $u(t,x)$ as a function of maturation x (full line) for $\tau = 0.2 < \tau_4 \simeq 0.46$, and for four increasing times $t = 0$ (full line), $t = 10$ (dash-dotted line), $t = 20$ (dash-triple dotted line) and $t = 40$ (dotted line). Whenever $\tau > \tau_4$ fronts will not propagate and the initial perturbation decays. At $x = 1$, due to the large delay the birth rate $\Gamma(u_\tau)$ is insufficient to arrest the "wash out" effect due to convection.

increases, the wave length of the oscillation decreases.

In partial summary, this section has shown that increasing the delay τ decreases the front velocity, and that for sufficiently large delays the fronts are oscillatory. The selection of the oscillation wave length is dictated by the length scale of the front, with steeper fronts giving shorter wave lengths. As the front propagates towards $x = 0$ it steepens and the structure of the population wake is refined.

4.3.4. Perturbation dissipation and strong delays

If $\tau > \tau_4 \simeq 0.46$ fronts do not propagate, the initial perturbation is dissipated, and the solutions evolve towards U_0.

Fig. 16 shows the cell density $u(t,x)$ as a function of maturation x, for $\tau = 1 > \tau_4 \simeq 0.46$. The figure shows that large delays produce a birth rate that can not sustain growth. Thus although an increase in the strength of delay refines the structure of the front solution, there is a threshold above which insufficient growth occurs. More quantitatively for the present case the initial growth rate at $x = 1$ is given by

$$\begin{aligned} \Gamma_{\text{init}} &= \Gamma(u(0, e^{-\tau})) \\ &= u(0, e^{-\tau})[1 - u(0, e^{-\tau})], \end{aligned} \tag{55}$$

which, for the parameters used here, gives $\Gamma_{\text{init}} = 4.53 \times 10^{-5}$. On the other hand, the initial convection effect $C = rx(\partial u/\partial x)$ at $x = 1$ is given by:

$$C = r\left[x\frac{\partial u}{\partial x}\right]_{x=1} = rp, \tag{56}$$

where we used the initial condition (10) for fronts. For the selected parameters the convection effect is $C = 0.1 \gg \Gamma_{\text{init}}$, and is sufficiently larger than the reaction rate to dissipate the front and drive the population towards the zero amplitude solution U_0.

5. Conclusions

Cell population models consisting of first order partial differential equations with temporal and spatial retardations were previously shown to predict a rich variety of phenomena. In this paper we have shown that a simplification of the more complex model of [4], containing only

spatial retardations, displays an interesting family of pulse and front propagation solutions depending on the magnitude of the spatial delay and the initial function. On the unit maturation interval single or multiple pulses propagate according to the magnitude of the non-local action. Fronts propagate and are monotonic if the delay is sufficiently small, but become oscillatory above a certain delay threshold. Scaling was found to be a useful tool to complement numerical simulations in obtaining the thresholds for various regime transitions.

It is well known that differential delay equations may display a multiplicity of solution types as the initial function is changed (cf. [16–20]). A change of variables $X = \log x$ in the equation

$$\frac{\partial u}{\partial t} + rx\frac{\partial u}{\partial x} = \mathcal{F}(u(t, x), u(t-\tau, \beta x)), \quad x \in [0, 1], \tag{57}$$

yields the equivalent equation

$$\frac{\partial g}{\partial t} + r\frac{\partial g}{\partial X} = \mathcal{F}(g(t, X), g(t-\tau, X-\bar{\tau})), \quad X \in (-\infty, 0], \tag{58}$$

where $g(t, X) = u(t, x)$ and $\bar{\tau} = -\log \beta$.

A casual examination of Eq. (58) seems to indicate that it is "simpler" than Eq. (57) from which it is derived, but in fact the transformation has made it effectively intractable to numerical analysis because of the infinite domain of X. Nevertheless, the transformation points out that the net effect of linear convection velocities (rx) in the original equation (57) is to compress the length scale of any pattern formation phenomena that occurs in the low maturation range (i.e., for $x \to 0$). For example, a train of propagating (moving) pulses will have a characteristic pulse-to-pulse distance that increases with increasing x, and a transient oscillatory front moving toward $x \to 0$ will continuously refine its wave length as it invades the smaller maturation ranges. The analysis of this effect of the maturation dependent convection and spatial nonlocality was the subject of Section 3, accomplished through a scaling analysis.

The transformation from Eq. (57) to (58) also points out that it is also not especially surprising that multiple solution types arise in the equation studied here. What is surprising is the varied nature of these solutions relative to the non-delayed and non-local versions studied in [8–13]. The richness of these solution types strong suggests that relatively simple functional partial differential equations may serve as simple prototypes for the modeling of complex wave phenomena. The challenge to the mathematician in formulating a proper theory of these behaviors is clear.

Acknowledgments

We thank the McGill University Computing Center for a grant to defray the computational costs of this research and the Natural Sciences and Engineering Research Council (Canada) for Operating Grant support to both A.D.R. and M.C.M. M.C.M. also thanks NATO, the Royal Society of London, and the Alexander von Humboldt Stiftung for support.

References

[1] M.C. Mackey and J.G. Milton, Comm. Theor. Biol. 1 (1990) 299.
[2] A.D. Rey and M.C. Mackey, Chaos 2 (1992) 231.
[3] A.D. Rey and M.C. Mackey, Canad. Appl. Math. Quart. 1 (1993) 61.
[4] M.C. Mackey and R. Rudnicki, J. Math. Biol. (1994) in press.
[5] A.D. Rey and M.C. Mackey, Physica D 80 (1994) 120–139.
[6] B. Finlayson, Numerical Methods for Problems with Moving Fronts (Ravena Park, Washington, 1992).
[7] M.C. Cross and P.C. Hohenberg, Rev. Mod. Phys. 65 (1993) 851.
[8] A. Lasota, Nonlin. Anal. 5 (1981) 1181.
[9] P. Brunovsky, Nonlin. Anal. 7 (1983) 167.
[10] P. Brunovsky and J. Komornik, J. Math. Anal. Appl. 104 (1984) 235.

[11] R. Rudnicki, Ergod. Theor. Dynam. Syst. 5 (1985) 437.
[12] R. Rudnicki, Bull. Pol. Acad. Sci. Math. 35 (1987) 289.
[13] K. Loskot, J. Diff. Eqns. 58 (1985) 1.
[14] J.A. Sherratt, Physica D 70 (1994) 370.
[15] V.I. Karpman, Non-linear Waves in Dispersive Media (Pergamon, Oxford, 1975).
[16] P. Dormayer, J. Diff. Eqns. 82 (1989) 109.
[17] P. Dormayer, Diff. Int. Eqns. 5 (1992) 831.
[18] J. Losson, M.C. Mackey and A. Longtin, Chaos 3 (1993) 167.
[19] R. Nussbaum, J. Diff. Eqns. 34 (1979) 25.
[20] H.-O. Walther, Contemp. Math. 129 (1992) 177.